blood

American Society of Hematology
2021 L Street NW, Suite 900,
Washington, DC 20036
Phone: 202-776-0544 | Fax 202-776-0545
editorial@hematology.org

RUNX1 isoform disequilibrium promotes the development of trisomy 21 associated myeloid leukemia

Tracking no: BLD-2022-017619R1

Sofia Gialesaki (Hannover Medical School, Germany) Daniela Bräuer-Hartmann (Martin Luther University Halle-Wittenberg, Germany) Hasan Issa (Goethe University Frankfurt, Germany) Raj Bhayadia (Goethe University Frankfurt, Germany) Oriol Alejo-Valle (Martin Luther University Halle-Wittenberg, Germany) Lonneke Verboon (Goethe University Frankfurt, Germany) Anna-Lena Schmell (Goethe University Frankfurt, Germany) Stephanie Laszig (Goethe University Frankfurt, Germany) Eniko Regenyi (Pediatric Hematology and Oncology, Martin-Luther-University Halle-Wittenberg, Germany) Konstantin Schuschel (Goethe University Frankfurt, Germany) Maurice Labuhn (Pediatric Hematology and Oncology, Hannover Medical School, Germany) Michelle Ng (Martin Luther University Halle-Wittenberg, Germany) Robert Winkler (Goethe University Frankfurt, Germany) Christian Ihling (Martin-Luther-University Halle-Wittenberg, Germany) Andrea Sinz (Martin-Luther-University Halle-Wittenberg, Germany) Markus Glaß (Martin Luther University Halle-Wittenberg, Germany) Stefan Hüttelmaier (Martin Luther University Halle-Wittenberg, Germany) Sören Matzk (Max-Planck-Institute for Molecular Genetics Berlin, Germany) Lena Schmid (Hannover Medical School, Germany) Farina Strüwe (Hannover Medical School, Germany) Sofie-Katrin Kadel (Hannover Medical School, Germany) Dirk Reinhardt (University Childrens Hospital Essen, Germany) Marie-Laure Yaspo (Max Planck Institute for Molecular Genetics, Germany) Dirk Heckl (Martin-Luther-University Halle-Wittenberg, Germany) Jan-Henning Klusmann (Goethe University Frankfurt, Germany)

Abstract:
Gain of chromosome 21 (Hsa21) is among the most frequent aneuploidies in leukemia. However, it remains unclear how partial or complete amplifications of Hsa21 promote leukemogenesis and why children with Down syndrome (i.e. trisomy 21) are particularly at risk of leukemia development. Here, we propose that *RUNX1* isoform disequilibrium with *RUNX1A* bias is key to Down syndrome-associated myeloid leukemia (ML-DS). Starting with Hsa21-focused CRISPR-Cas9 screens, we uncovered a strong and specific *RUNX1* dependency in ML-DS cells. Expression of the *RUNX1A* isoform is elevated in ML-DS patients, and mechanistic studies using murine ML-DS models and patient-derived xenografts (PDXs) revealed that excess RUNX1A synergizes with the pathognomonic *Gata1s* mutation during leukemogenesis by displacing RUNX1C from its endogenous binding sites and inducing oncogenic programs in complex with the MYC cofactor MAX. These effects were reversed by restoring the RUNX1A:RUNX1C equilibrium in PDXs *in vitro* and *in vivo*. Moreover, pharmacological interference with MYC:MAX dimerization using MYCi361 exerted strong anti-leukemic effects. Thus, our study highlights the importance of alternative splicing in leukemogenesis, even on a background of aneuploidy, and paves the way for the development of specific and targeted therapies for ML-DS, as well as for other leukemias with Hsa21 aneuploidy or *RUNX1* isoform disequilibrium.

Conflict of interest: COI declared - see note

COI notes: D.R. has advisory roles for Celgene Corporation, Novartis, Bluebird Bio, Janssen, and receives research funding from CLS Behring and Roche. J.H.K. has advisory roles for Bluebird Bio, Novartis, Roche and Jazz Pharmaceuticals. M.L.Y. is partially employed by Alacris Theranostics.

Preprint server: Yes; BioRxiv https://doi.org/10.1101/2022.03.07.483334

Author contributions and disclosures: S.G. and D.B.H. performed experiments, analyzed and interpreted data and revised the manuscript. R.B., O.A.V., H.I., M.L., C.I., L.S, F.J.S. and S.K.K. performed experiments and analyzed data. E.R., M.G., S.M. and M.N. performed bioinformatics analysis and data interpretation, and revised the manuscript. A.S., S.H., M.L.Y. supervised the analyses and revised the manuscript. D.R. provided patient material and data. D.H. and J.H.K. designed the study, analyzed and interpreted data, wrote the manuscript and academically drove the project.

Non-author contributions and disclosures: No;

Agreement to Share Publication-Related Data and Data Sharing Statement: RNA-Seq gene expression data have been deposited in the European Nucleotide Archive (ENA) and are accessible through accession numbers: ERS6071576 - ERS6071595. CUT&RUN data are accessible through ENA with the accession numbers: ERS5956460 - ERS5956467. Mass spectrometry proteomics data have been deposited to the ProteomeXchange Consortium via the PRIDE partner repository with the dataset identifier identifier PXD030616 and 10.6019/PXD030616. Data will be available immediately following publication, no end date. Other remaining data are available within the Article and Supplementary Files, or from the authors upon request.

Clinical trial registration information (if any):

RUNX1 isoform disequilibrium promotes the development of trisomy 21 associated myeloid leukemia

Sofia Gialesaki[1]*, Daniela Braeuer-Hartmann[2]*, Hasan Issa[3], Raj Bhayadia[3], Oriol Alejo-Valle[2], Lonneke Verboon[3], Anna-Lena Schmell[3], Stephanie Laszig[3], Enikő Regenyi[2,4], Konstantin Schuschel[3], Maurice Labuhn[1], Michelle Ng[2], Robert Winkler[3], Christian Ihling[5], Andrea Sinz[5], Markus Glaß[6], Stefan Hüttelmaier[6], Sören Matzk[4], Lena Schmid[1], Farina Josepha Strüwe[1], Sofie-Katrin Kadel[1], Dirk Reinhardt[7], Marie-Laure Yaspo[4], Dirk Heckl[2#], Jan-Henning Klusmann[3,8,9#]

[1]Pediatric Hematology and Oncology, Hannover Medical School, Hannover, Germany

[2]Pediatric Hematology and Oncology, Martin-Luther-University Halle-Wittenberg, Halle, Germany

[3]Department of Pediatrics, Goethe-University Frankfurt, Frankfurt, Germany

[4]Max Planck Institute for Molecular Genetics, Berlin, Germany

[5]Department of Pharmaceutical Chemistry and Bioanalytics, Institute of Pharmacy, Martin-Luther-University Halle-Wittenberg, Halle, Germany

[6]Institute of Molecular Medicine, Martin-Luther-University Halle-Wittenberg, Halle, Germany

[7]Pediatric Hematology and Oncology, Pediatrics III, University Hospital Essen, Germany.

[8]Frankfurt Cancer Institute, Goethe University Frankfurt, Frankfurt am Main, Germany

[9]German Cancer Consortium (DKTK), Partner Site Frankfurt/Mainz and German Cancer Research Center (DKFZ), Heidelberg, Germany

*These authors contributed equally

#These authors contributed equally

Running Title: *RUNX1* isoforms in trisomy 21 associated leukemia

Keywords: Acute Myeloid Leukemia, Down syndrome, Trisomy 21, RUNX1, GATA1

Corresponding authors: Prof. Dr. Jan-Henning Klusmann, E-mail: jan-henning.klusmann@kgu.de, Tel.: +496960315094; Dirk Heckl (Dirk.Heckl@uk-halle.de), Tel.: +493455577273.

Lead contact author: Jan-Henning Klusmann

Scientific category: Hematopoiesis and stem cells
Abstract word count: 200
Text word count: 4264
Figure/table count: 6

Reference count: 59

Key points

- *RUNX1* isoform disequilibrium towards *RUNX1A* and its interaction with MYC:MAX is key to the pathogenesis of trisomy 21-associated myeloid leukemia
- Restoration of RUNX1A:RUNX1C equilibrium and pharmacological interference with MYC:MAX dimerization reverses the oncogenic phenotype

Abstract

Gain of chromosome 21 (Hsa21) is among the most frequent aneuploidies in leukemia. However, it remains unclear how partial or complete amplifications of Hsa21 promote leukemogenesis and why children with Down syndrome (i.e. trisomy 21) are particularly at risk of leukemia development. Here, we propose that *RUNX1* isoform disequilibrium with *RUNX1A* bias is key to Down syndrome-associated myeloid leukemia (ML-DS). Starting with Hsa21-focused CRISPR-Cas9 screens, we uncovered a strong and specific *RUNX1* dependency in ML-DS cells. Expression of the *RUNX1A* isoform is elevated in ML-DS patients, and mechanistic studies using murine ML-DS models and patient-derived xenografts (PDXs) revealed that excess RUNX1A synergizes with the pathognomonic *Gata1s* mutation during leukemogenesis by displacing RUNX1C from its endogenous binding sites and inducing oncogenic programs in complex with the MYC cofactor MAX. These effects were reversed by restoring the RUNX1A:RUNX1C equilibrium in PDXs *in vitro* and *in vivo*. Moreover, pharmacological interference with MYC:MAX dimerization using MYCi361 exerted strong anti-leukemic effects. Thus, our study highlights the importance of alternative splicing in leukemogenesis, even on a background of aneuploidy, and paves the way for the development of specific and targeted therapies for ML-DS, as well as for other leukemias with Hsa21 aneuploidy or *RUNX1* isoform disequilibrium.

Introduction

Major multi-omic efforts have mapped the cytogenetic, mutational and epigenetic landscape of many cancers, including acute myeloid leukemia (AML) [1,2]. Subsequent functional studies involving disease modeling in mice or in human cells have pointed towards complex cooperation between common fusion oncogenes and recurrently mutated genes during disease initiation and progression. However, the contribution of aneuploidy to oncogenesis remains poorly understood [3], due to context-dependent effects, technical challenges, and a lack of appropriate models. Chromosome 21 (Hsa21) gain – one of the most frequent numerical alterations in leukemia [4,5] – is no exception.

Myeloid leukemia associated with Down syndrome (ML-DS) and its preleukemic predecessor, transient abnormal hematopoiesis (TAM), are excellent paradigms for studying leukemic progression associated with trisomy 21. TAM is caused by a single genetic mutation in the transcription factor GATA1 in trisomic fetal stem and/or progenitor cells, which causes the exclusive expression of a shorter isoform known as GATA1s [6]. We and others have shed light on the additional mutational events that are required for progression to overt ML-DS [7,8], however, far less is known about the role of trisomy 21 in creating the TAM/ML-DS disease phenotype. A critical region has been identified on Hsa21 that mediates the expansion of early hematopoietic progenitors observed in DS patients [9-11] and several Hsa21 genes – such as *ERG* [12,13], *DYRK1A* [14], *CHAF1B* [15] and miR-125b [16,17] – have been postulated to play a role in leukemogenesis. On the other hand, Ts65dn mice that are trisomic for 104 orthologs of Hsa21 genes do not fully recapitulate the human phenotype in association with *GATA1s* [18], and the postulated factors are either located outside of the critical region, not overexpressed in

trisomic fetal progenitor cells [11], or lack full leukemic potential in humans when combined with mutated *GATA1s* [14,19,20].

The transcription factor RUNX1, which is essential for the establishment of definitive hematopoiesis [21-23], has attracted considerable attention as a candidate Hsa21 oncogene. While RUNX1 has been extensively studied in leukemia development [24,25], its expression is reduced in trisomic fetal progenitor cells [11] and its trisomy is dispensable for myeloproliferative disease in elderly Ts65dn mice [24]. Despite early hints pointing towards differential roles for alternatively spliced *RUNX1* isoforms in ML-DS[26], studies to date have not accounted for the fact that *RUNX1* is transcribed from two distinct promoters and undergoes alternative splicing, giving rise to three main isoforms with diverse effects on hematopoiesis [27]: *RUNX1C* – transcribed from the P1 promoter – is the most abundant isoform in definitive hematopoiesis. *RUNX1A* and *RUNX1B* – both transcribed from the P2 promoter – are differentially expressed throughout hematopoietic differentiation [28-30]. Interestingly, due to the lack of a splice acceptor site in an isoform-specific exon, mice do not express *RUNX1A* – the short *RUNX1* isoform that lacks the transactivation domain – underlining important species-specific differences [31], and contributing in part to the incomplete understanding of isoform-specific roles for RUNX1.

In this study, we systematically investigated protein coding genes on Hsa21 for dependency in ML-DS, and found that disequilibrium of the *RUNX1* isoforms – and specifically, excess *RUNX1A* – is key to trisomy 21-associated leukemogenesis.

Methods

Reagents and Resources

Supplemental Table 1 contains a list of all relevant reagents.

Patient samples

Pediatric AML samples were collected from patients enrolled in the AML Berlin-Frankfurt-Münster treatment protocols for children and adolescents. Written informed consent was obtained from all patients and custodians in accordance with the Declaration of Helsinki and local laws and regulations, and the study was approved by the institutional review boards of all participating centers. For details, see **Supplemental Table 2**.

Animal studies

All animal experiments were performed according to protocols approved by the local authorities (*Niedersächsisches Landesamt für Verbraucherschutz und Lebensmittelsicherheit, Landesverwaltungsamt Sachsen-Anhalt* and *Regierungspräsidium Darmstadt*). The animals were maintained under pathogen-free conditions.

Statistical analysis

Statistical evaluation was performed using Student's t-tests, Mann-Whitney tests, and one-way or two-way ANOVA. The Kaplan-Meier method and log-rank tests were used to estimate overall survival and to compare differences between survival curves, respectively. All data are presented as mean ± standard deviation (SD). Calculations

were performed using GraphPad Prism 8/9 (STATCON). All statistical tests and sample numbers are disclosed in the respective figure legends/supplementary tables.

Data availability

RNA-Seq gene expression data have been deposited in the European Nucleotide Archive (ENA) and are accessible through accession numbers: ERS6071576 - ERS6071595. CUT&RUN data are accessible through ENA with the accession numbers: ERS5956460 - ERS5956467. Mass spectrometry proteomics data have been deposited to the ProteomeXchange Consortium via the PRIDE partner repository with the dataset identifier identifier PXD030616 and 10.6019/PXD030616. Data will be available immediately following publication, no end date. Other remaining data are available within the Article and Supplementary Files, or from the authors upon request.

Additional detailed methods can be found in the **Supplemental Methods.**

Results

CRISPR-Cas9 screen reveals RUNX1 dependency in ML-DS

In order to identify potential oncogenes on Hsa21 that contribute to the pathogenesis of TAM and ML-DS, we generated a lentiviral CRISPR-Cas9 library (1090 sgRNA) targeting the 218 annotated coding genes on Hsa21 and performed a dropout screen in the ML-DS cell line CMK, as well as in the erythroleukemia cell line K562 (**Figure 1A**). We identified 19 genes specifically required for the survival of CMK cells (**Figure 1B** and **Supplemental Table 3**). Interestingly, we observed a strong depletion of *RUNX1*-targeting sgRNAs in CMK but not K562 cells (**Figure 1B-C**). Subsequent flow cytometry-based depletion assays using individual sgRNAs found *RUNX1* to be the most specific ML-DS dependency in our screen, with the sgRNAs' impact on cell survival corresponding to RUNX1 knockdown levels (**Figure 1C** and **Supplemental Figure 1A-D**). These results were recapitulated in stable Cas9-expressing ML-DS patient-derived blasts *in vitro* and in fluorescence-based competitive transplantation assays *in vivo* (**Figure 1C-E, Supplemental Figure 1E-G** and **Supplemental Table 2**).

Considering that former studies have disputed the role of *RUNX1* in TAM/ML-DS pathogenesis, and given that Bourquin et al. hypothesized that alternatively spliced *RUNX1* isoforms may lead the reduced expression of RUNX1 targets in ML-DS,[11,24,26] we wondered whether deregulation of the *RUNX1* isoforms may underlie its dependency phenotype in ML-DS cells, rather than altered overall expression. Nanopore full length RNA sequencing revealed that the main isoforms – *RUNX1A*, *RUNX1B* and *RUNX1C* – are predominant in TAM and ML-DS (**Figure 1F**). We thus further quantified the expression of these 3 isoforms in healthy hematopoietic cells (HSPCs, erythrocytes, megakaryocytes, granulocytes and monocytes) and TAM/ ML-DS blasts. *RUNX1C* is the

predominant isoform in all cell types, but ML-DS and trisomy 21 samples presented with elevated expression of the *RUNX1A* isoform, resulting in a significantly higher *RUNX1A*:*RUNX1B/C* ratio compared to HSPCs or terminally differentiated cells (**Figure 1G** and **Supplemental Figure 1H-K**).

Notably, trisomy 21 is associated with an elevated *RUNX1A*:*RUNX1B/C* ratio, as determined by comparing fetal trisomy 21 and non-trisomic $CD34^+$ HSPCs (**Supplemental Figure 1H-I)**. Interestingly, this imbalance can be induced by elevated levels of the splicing factor subunit U2AF1, which is encoded by chromosome 21 (**Supplemental Figure 2A**). Moreover, GATA1s' ability to regulate *RUNX1* isoforms appears to be impaired compared to full-length GATA1. It shows reduced occupancy at the RUNX1 P1 und P2 promoter regions in *Gata1s*-FLCs (**Supplemental Figure 2B-D**) and causes higher *RUNX1A* levels in CRISPR-Cas9 edited human megakaryocytic / erythroid precursors cultured *in vitro* compared to wild-type controls (**Supplemental Figure 2E**). Induced expression of *GATA1* and *GATA1s* in K562 cells activated transcription from the P2 promoter, leading to increased *RUNX1A* and *RUNX1B* expression, whereas *RUNX1C* transcription from the P1 promoter was enhanced by *GATA1* but repressed by *GATA1s* (**Supplemental Figure 2F**). Altogether these data suggest a mechanism where trisomy 21 and *GATA1s* synergize to amplify *RUNX1* isoform imbalance.

Thus, our CRISPR-Cas9 screen of Hsa21 genes and subsequent *RUNX1* isoform expression analyses in patient samples suggest that *RUNX1* isoform disequilibrium and *RUNX1A* bias contribute to the pathogenesis of TAM and ML-DS.

Increased RUNX1A:RUNX1C ratio induces malignant ML-DS phenotype

To probe the functional relevance of unbalanced *RUNX1* isoform expression in TAM and ML-DS development, we modulated the *RUNX1A*:*RUNX1C* ratio in fetal and neonatal $CD34^+$ HSPCs of human origin and in patient-derived ML-DS blasts (**Supplemental Figure 3A**). Methylcellulose-based CFU assays showed the sustained growth of *RUNX1A*-expressing $CD34^+$ HSPCs, as evidenced by increased replating capacity (**Figure 2A**). In culture conditions promoting megakaryocytic differentiation, *RUNX1A* expression induced the expansion of $CD34^+$ immature cells and blocked their differentiation to $CD41^+/CD61^+CD42b^+$ megakaryocytes (**Figure 2B-C** and **Supplemental Figure 3B**) – effects that were more pronounced in fetal cells and that we confirmed in collagen-based megakaryocytic colony-forming (CFU-Mk) assays (**Supplemental Figure 3C**). To better understand the effects of *RUNX1A* and *RUNX1C* on lineage fate decision, we additionally cultured $CD34^+$ HSPCs in conditions allowing for differentiation along the erythroid as well as megakaryocytic lineages. *RUNX1C* and *RUNX1A* conferred a lineage bias towards megakaryopoiesis ($CD41^+/CD235a^-$) over erythropoiesis ($CD41^-/CD235a^+$) in neonatal $CD34^+$ HSPCs. *RUNX1A* halted cells in an undifferentiated $CD117^+$ stage (**Supplemental Figure 3D-E**).

Importantly, restoring the *RUNX1A*:*RUNX1C* equilibrium through *RUNX1C* expression in ML-DS patient-derived blasts (**Supplemental Figure 3A**) halted proliferation and accelerated differentiation, as indicated by loss of CD117 and gain of CD33 and CD41 expression (**Figure 2D-F**). Inversely, further increasing the expression of *RUNX1A* conferred a mild growth advantage in ML-DS blasts and increase in the fraction of cells with an immature phenotype ($CD33^+CD117^+$ or $CD41^+CD42b^-CD117^+$ myeloid/megakaryocytic blasts; **Figure 2D-F**). Lastly, we evaluated restoration of

RUNX1A:*RUNX1C* ratio *in vivo* through fluorescence-based competitive transplantation assays using two ML-DS patient-derived xenografts (PDX; **Figure 2G**). In both cases, *RUNX1C*-expressing leukemic blasts were significantly diminished in the bone marrow of recipient mice at the experimental endpoint, whereas *RUNX1A*-expressing leukemic blasts were unchanged compared to control-transduced blasts (**Figure 2H**).

In summary, these experiments in primary human cells depict a landscape of perturbed differentiation and accelerated proliferation guided by *RUNX1A*. Our data further demonstrate that restoring *RUNX1A:RUNX1C* equilibrium can overcome differentiation arrest in ML-DS blasts, leading to their depletion.

RUNX1A synergizes with *Gata1s* in the leukemic transformation of fetal liver cells

As TAM occurs *in utero*, implying a fetal origin for this disease, we employed a murine fetal liver cell (FLC)-based *in vitro* model to study the oncogenic potential of *RUNX1* isoform imbalance in concert with mutated *Gata1s* [7] (**Supplemental Figure 3A**). Notably, mice do not express the *RUNX1A* isoform [31], underlining important species-specific differences that could explain the inability of previous Down syndrome mouse models to recapitulate the human TAM/ML-DS phenotype [18,32]. Combined lentiviral transduction of Cas9-knock-in FLCs with *RUNX1A* and a sgRNA targeting exon 2 of *Gata1* – thereby introducing *Gata1s* mutations – indeed resulted in a robust hyperproliferative phenotype (4140-fold; **Figure 3A**) compared to cells transduced with a combination of a non-targeting control sgRNA (sgCtrl) and empty vector (EV). Individually, *Gata1s* (sgGata1+EV) and *RUNX1A* expression (sgCtrl+*RUNX1A*) also enhanced growth (**Figure 3A**; 366-fold and 140-fold, respectively), but the effect was less pronounced than in combination, suggesting synergy between *Gata1s* and

RUNX1A. Inversely, ectopic expression of *RUNX1C* or *RUNX1B* alone or in combination with *Gata1s* mutations resulted in a growth disadvantage (**Figure 3A** and **Supplemental Figure 4A**). We note that none of the other Hsa21 candidate genes selected from our sgRNA dropout screen produced a synergistic hyperproliferative phenotype with *Gata1s* (**Supplemental Figure 4B**). Immunophenotypically, the hyperproliferative *RUNX1A Gata1s*-FLCs were $CD117^{+}CD41^{+}$ and partially $CD71^{+}Ter119^{+}$ (**Figure 3B**), corresponding to megakaryocytic progenitors with erythroid features – a hallmark of TAM/ML-DS. The expression of erythroid markers was increased upon *RUNX1A* expression compared to control *Gata1s*-FLCs (**Figure 3B**). The synergistic effect of *RUNX1A* and *Gata1s* on the proliferation of FLCs was also observed in culture conditions promoting the expansion and differentiation of erythroid progenitor cells, but not in conditions promoting myeloid expansion and differentiation (**Supplemental Figure 4C**).

Comparative transcriptomic analysis of RNA-sequencing (RNA-seq) data substantiated the synergy between *Gata1s* mutations and *RUNX1A* expression. As previously described, gene set enrichment analysis (GSEA) revealed a marked reduction of erythroid genes and concurrent activation of pro-proliferative genes – including MYC and E2F targets – in *Gata1s* mutated FLCs (**Figure 3C-D** and **Supplemental Table 4**) [16,18,33]. While *RUNX1A* expression mitigated the reduction of erythroid genes caused by *Gata1s*, it triggered a similar upregulation of MYC and E2F target genes, suggesting convergence on these oncogenic pathways. In addition, *RUNX1A* expression in the background of *Gata1s* induced target genes of EVI1 – one of the most invasive proto-oncogenes in human leukemia [34]– and a long-term hematopoietic stem cell signature, whereas the opposite was true upon *RUNX1C* expression (**Figure 3D-E** and

Supplemental Table 4). Hence, the synergistic oncogenic expression program of *Gata1s* and *RUNX1A* is characterized by the induction of EVI1, MYC and E2F genes target genes, and a long-term hematopoietic stem cell signature, and the concomitant repression of erythroid and megakaryocytic differentiation signatures.

To further explore the leukemogenic potential of *RUNX1* isoform disequilibrium in the pathogenesis of Down syndrome-associated leukemia, we performed *in vivo* experiments using *Gata1s*-FLCs. Upon transplantation into sub-lethally irradiated syngeneic recipients (C57Bl/6J), *Gata1s*-FLCs typically become transiently abundant in the peripheral blood [7]. In contrast, *RUNX1A*-expressing *Gata1s*-FLCs caused high penetrance (100%) leukemia with a short latency (median survival: 39 days) and organ infiltration (**Figure 3F-G** and **Supplemental Figure 4D**). Detailed flow cytometry analysis revealed cells of a megakaryocytic progenitor-like phenotype ($CD41^+CD117^+CD34^-CD16/32^{low}$) resembling TAM and ML-DS (**Figure 3H** and **Supplemental Figure 4E**), which re-initiated disease when transplanted into secondary recipients (**Supplemental Figure 4F**). Notably, *RUNX1A* expression did not cause leukemia in wild-type *Gata1*-FLCs (**Supplemental Figure 4G**). Transcriptomic analysis of RNA-seq data from the murine leukemias in comparison to stringently sorted murine fetal liver stem and/or progenitor populations confirmed the megakaryocytic progenitor-like phenotype and the ML-DS-like gene expression profile [26,35] (**Figure 3I-J** and **Supplemental Table 5**). Importantly, Cre recombinase-mediated excision of the LoxP-flanked *RUNX1A* cDNA induced rapid depletion of the leukemic blasts *in vitro*, underlining their dependency on *RUNX1A* and its importance in ML-DS pathogenesis (**Supplemental Figure 4H**). Of note, miR-125 further accelerated the leukemic transformation of *Gata1s*-FLCs by *RUNX1A,* suggesting synergy between RUNX1A and

another well characterized oncogene on chromosome 21 [16,36] (**Supplemental Figure 4I**).

These data demonstrate that the interplay between *Gata1s* and *RUNX1* isoform disequilibrium results in the proliferation and accumulation of immature megakaryocytic progenitors *in vitro*, and in ML-DS-like leukemia or an aggressive form of TAM *in vivo*.

Distinct RUNX1A and RUNX1C protein interaction networks

To better understand the oncogenic mechanisms mediated by RUNX1A in TAM/ML-DS, we compared RUNX1A and RUNX1C protein interaction networks via co-immunoprecipitation of doxycycline-inducible HA-tagged RUNX1A and RUNX1C in CMK cells, followed by mass spectrometry of the bound cofactors (**Figure 4A** and **Supplemental Figure 5A**). 98 and 57 proteins were significantly bound by RUNX1C and RUNX1A, respectively (**Figure 4B** and **Supplemental Figure 5B-C**). Of these, 45 proteins were commonly bound by both RUNX1 isoforms, including CBFβ and other *bona fide* RUNX1 interaction partners. 53 protein interactions were unique to RUNX1C. RUNX1C-specific cofactors were enriched for proteins involved in the regulation of cell cycle, gene expression, protein and mRNA metabolism as well as chromosome organization (**Figure 4B**). Interestingly, members of the spliceosome A/C and NSL complexes (e.g. SF3B1, WDR5 and KANSL2) were among the RUNX1C-specific cofactors (**Supplemental Figure 5D**), suggesting an active role in splicing and chromosomal organization that is lost in RUNX1A, as demonstrated for the RUNX1::RUNX1T1 fusion oncoprotein [37]. In contrast, the 12 RUNX1A-specific cofactors are involved in active transcription/replication and G1-S transition, including the megakaryocytic transcription factor NFE2, which is mutated in a subset of patients with

myeloid neoplasms and is functionally involved in the megakaryocyte differentiation blockage of *GATA1s* pluripotent stem cells [38,39,40](**Figure 4B**). Importantly, MAX – a crucial cofactor of MYC – was among the RUNX1A-specific interacting proteins, as verified via Western blot (**Figure 4C**). GATA1s co-immunoprecipitated with RUNX1A and RUNX1C, albeit not at a significant enrichment level (data not shown). As GATA1 is a well-described RUNX1 interaction partner [41] and as *GATA1s* mutations characterize TAM/ML-DS [42,43], we investigated their putative differential binding of RUNX1A and RUNX1C in more detail. To this end, we pulled down doxycycline-induced HA-tagged GATA1 or GATA1s in stably transduced CMK cells, which harbor endogenous *GATA1s* mutations and hence exclusively express GATA1s. This is an important point, since GATA1 forms homodimers [44,45] precluding the enrichment of GATA1s-specific protein complexes in the presence of GATA1. We found that both GATA1 and GATA1s interact with RUNX1C, as previously described [46]. However, neither GATA1 nor GATA1s appear to interact with RUNX1A (**Figure 4D**). Thus, our proteomic data suggest an altered protein interaction network, which may contribute to the TAM/ML-DS specific phenotype of RUNX1A in *GATA1*-mutated cells.

RUNX1A affects gene regulation by displacing endogenous RUNX1C

To further interrogate the RUNX1A-centered protein interaction network and determine the consequences of its inability to form a complex with GATA1 or GATA1s, we performed CUT&RUN on endogenous GATA1s and RUNX1C (using a C-terminal antibody that does not recognize exogenous RUNX1A) in *Gata1s*-FLC with or without exogenous expression of doxycycline-inducible HA-tagged RUNX1A or RUNX1C (**Figure 5A** and **Supplemental Figure 6A**). We found that 33% of the promoter or

enhancer regions occupied by endogenous RUNX1C were also occupied by HA-RUNX1A, and that half (52%) of the RUNX1C/RUNX1A occupied regulatory regions were co-bound by GATA1s (**Figure 5B** and **Supplemental Table 6**)**,** corroborating the known GATA1-RUNX1 interplay in transcriptional regulation [47].

Unsupervised clustering of peaks at regulatory regions bound by endogenous RUNX1C, GATA1 and HA-RUNX1A revealed three clusters (**Figure 5C**). *De novo* motif discovery uncovered an enrichment of RUNX family motifs in clusters 1 and 3, whereas GATA family motifs were most abundant in cluster 2 (**Supplemental Figure 6B-C**). Importantly, we observed a global reduction of endogenous RUNX1 occupancy upon HA-RUNX1A expression across all clusters (**Figure 5D, Supplemental Figure 6D** and **Supplemental Table 6**). Consistent with our protein-protein interaction studies, GATA1s binding increased globally upon expression of HA-RUNX1C, in comparison to HA-RUNX1A and the empty vector control (**Figure 5D** and **Supplemental Figure 6E**).

Interestingly, the majority of the genes in the three CUT&RUN clusters were upregulated upon HA-RUNX1A expression (67.6-81.5%) (**Supplemental Figure 6C**). Transcription factor motif analysis of peaks in the promoter regions of differentially expressed genes revealed an overrepresentation of the MYC-coactivation factor E2F as well as of single MYC, MAX and MYC:MAX dimeric motifs (**Figure 5E** and **Supplemental Table 7**). The median distance between the RUNX1 and MYC:MAX binding motifs (under HA-RUNX1A peaks) was 298 bp. Among the RUNX1A-induced genes with MAX or MYC:MAX binding motifs in their promoter regions are *Mxd1* (*Mad1; Max Dimerization Protein 1*), *Myct1 (MYC target 1)*, known oncogenic drivers such as *Lyl1* and *Malat1* as well as the megakaryocyte gene *Itga2b* (CD41) – all of which were repressed by RUNX1C in RNA-seq experiments (**Figure 5F** and **Supplemental Figure 6F-H**). These

data are consistent with our comparative transcriptomic analyses in *Gata1s*-FLCs, which uncovered the activation of MYC and E2F targets by GATA1s and RUNX1A resulting in a synergistic induction of proliferation and an immature phenotype, while the opposite was true for *RUNX1C* (**Figure 3C-E**).

Taken together, our proteomic and genomic analyses imply that RUNX1A interferes with normal RUNX1C function by displacing it from target gene promoters. Instead, RUNX1A interacts with the MYC co-factor MAX and induces an MYC- and E2F-driven expression program. The concerted alteration of normal megakaryocytic progenitor gene expression programs through GATA1s and RUNX1A leads to malignant transformation in these cells, via the upregulation of oncogenic gene expression programs and the perturbation of RUNX1C-regulated differentiation programs, respectively.

Targeting MYC:MAX dimerization as a therapeutic approach for ML-DS

Finally, we investigated the role of the MYC co-factor MAX, which we hypothesized to be central to the synergy between GATA1s and RUNX1A, during leukemia pathogenesis. ShRNA-mediated knockdown and sgRNA-mediated knockout of *MAX* inhibited the growth of CMK cells *in vitro* (**Supplemental Figure 7A-B**). These findings were confirmed in murine *RUNX1A Gata1s*-FLCs and in ML-DS blasts derived from two patients (**Supplemental Figure 7C-F**). Normal $CD34^+$ HSPCs showed only a mild growth impairment upon *MAX* depletion (**Supplemental Figure 7G-H**). Importantly, pharmacological disruption of MYC:MAX dimerization using the MYC inhibitor MYCi361 [48] caused apoptotic cell death in *RUNX1A Gata1s*-FLCs and in CMK and K562 cells – which are *MYC*-dependent (**Figure 1B**) – in a dose dependent manner (**Figure 6A** and **Supplemental Figure 8A-B**). Accordingly, MYCi361 also induced apoptosis and partial

differentiation in ML-DS blasts derived from three patients, with median lethal concentration (IC_{50}) values of 2.09 μM, 2.63 μM and 3.82 μM, respectively (**Figure 6B** and **Supplemental Figure 8C**). Similarly, blasts derived from non-DS-AMKL and *KMT2Ar* patients – two other AML subgroups that have elevated *RUNX1A:RUNX1C* ratios (**Supplemental Figure 1H-K**) – also showed good responses with partial differentiation and median IC_{50} values between 3.9-4.32 μM and 3.9-5.88 μM, respectively (**Supplemental Figure 8D-H**). Normal $CD34^+$ HSPCs from two donors had IC_{50} values of 7.291 μM and 7.168 μM, respectively (**Supplemental Figure 8I-K**), outlining a therapeutic window. Lastly, we evaluated *MAX* knockdown *in vivo* through fluorescence-based competitive transplantation assays using ML-DS and AMKL patient-derived xenografts (PDX; **Figure 6C**). In both cases, *MAX*-depleted leukemic blasts were significantly diminished in the bone marrow of recipient mice at the experimental endpoint (**Figure 6D**).

Thus, we demonstrate that the MYC co-factor MAX is key to leukemic transformation mediated by RUNX1A and GATA1s, and that it can be therapeutically exploited.

Discussion

Aneuploidies, and in particular partial or complete amplifications of chromosome 21, are frequent alterations in leukemia; however, their underlying pathomechanisms remain enigmatic[3]. In this study, we leveraged the model system of Down syndrome-associated TAM and ML-DS to interrogate oncogenic factors on chromosome 21 for their roles in AML pathogenesis. A CRISPR-Cas9 screen of chromosome 21 genes unexpectedly revealed *RUNX1* as an ML-DS dependency in cell lines and patient-derived blasts *in vitro* and *in vivo*, despite former controversy regarding its role in TAM and ML-DS [3,24]. Through detailed functional validation, we discovered that, rather than *RUNX1* gene dosage, *RUNX1* isoform disequilibrium in the form of *RUNX1A* bias is key to trisomy 21-associated leukemogenesis. By dissecting the consequences of *RUNX1* disequilibrium in TAM/ML-DS, we showed that *RUNX1A* acts in concert with pathognomonic *GATA1s* mutations in this context, thereby blocking megakaryocytic differentiation and accelerating progenitor proliferation – effects that were reversed upon restoring the *RUNX1A*:*RUNX1C* equilibrium in murine models and patient-derived blasts *in vitro* and *in vivo*. These findings are in line with the known function of *RUNX1C* during adult hematopoiesis [49-51], where it regulates megakaryopoiesis by controlling the proliferation and survival of committed progenitors [52]. Thus, through the systematic interrogation of chromosome 21-encoded coding genes, our work contributes to understanding the synergy between trisomy 21 and *GATA1* mutations in ML-DS leukemogenesis. We suggest a model where *RUNX1A*:*RUNX1C* disequilibrium in TAM and ML-DS is a consequence of the combination of trisomy 21 and *GATA1s* mutations in fetal HSPCs. Our findings have further implications for other types of leukemia with numerical or structural alterations of chromosome 21 and/or *RUNX1* isoform disequilibrium: Indeed,

we also observed elevated *RUNX1A:RUNX1C* ratios in non-DS acute megakaryoblastic leukemia, *KMT2A*-rearranged AML and AML with complex karyotype (**Supplemental Figure 1E-K**). The exact mechanism leading to *RUNX1A:RUNX1C* dysregulation in trisomy 21 HSPCs remains an open question. One hypothesis is that altered transcriptional regulation by GATA1s and elevated levels of the Hsa21-encoded splicing factor *U2AF1* may combine to drive *RUNX1* isoform imbalance in TAM and ML-DS (**Supplemental Figure 2**); different mechanisms or mutations in splicing factors may be responsible in other subtypes of AML or myelodysplastic syndromes (MDS) [53]. In addition, RUNX1A may further enhance the oncogenic effect of miR-125b, another well-characterized oncogenic driver on chromosome 21 [16].

Mechanistically, we showed that the altered protein interaction network of RUNX1A (compared to RUNX1B/C) underlies its oncogenic function. RUNX1A fails to interact with GATA1 and GATA1s to control megakaryopoiesis [46]. Our proteomics analyses point towards RUNX1A's increased affinity for the MYC cofactor MAX. We propose a model where RUNX1A, in complex with MAX, displaces RUNX1C from its endogenous binding sites, where it normally recruits GATA1. Thus, RUNX1A perturbs RUNX1C:GATA1 regulated gene expression and activates MYC:MAX and E2F target genes, leading to a megakaryocytic differentiation block and acceleration of progenitor proliferation. This model would help explain the synergistic oncogenic effect of RUNX1A and GATA1s: GATA1s not only fails to repress *RUNX1A*, but also E2F and MYC target genes, during megakaryopoiesis [18], suggesting a double hit on these pathways in fetal trisomy 21 HSPCs. The central role of MAX in the RUNX1A-induced phenotype was validated by genetically interfering with *MAX* expression. Importantly, the dependency of ML-DS blasts on intact MAX represents a vulnerability that can be therapeutically exploited, as

we demonstrated by using the MYC:MAX dimerization inhibitor MYCi361 [48] to eradicate ML-DS patient blasts.

Although previous studies have reported the oncogenic and dominant negative effects RUNX1A exerts on RUNX1B [53-57], our findings are unexpected and have general implications for basic oncology research. First, our study demonstrates that species-specific differences in isoform expression must be considered when interpreting species-specific or divergent phenotypes in mouse models. *RUNX1A* is a primate-specific isoform of *RUNX1* [31], which may explain the inability of Down syndrome mouse models [32,58] to recapitulate the human TAM/ML-DS phenotype or the interplay of GATA1s and trisomy 21 seen in human induced pluripotent stem cells [3,11,19,59]. Second, our study underlines the importance of accounting for all isoforms when studying the oncogenic effects of a given gene and emphasizes the importance of alternative splicing in the pathogenesis of cancer. Various mutations in splicing factors have been identified in AML and MDS genomes [60]. Whether these mutations are causative for the increased RUNX1A:RUNX1B/C ratio observed in MDS [53] will need to be investigated in the future.

Overall, our study provides a general framework for interrogating the contribution of aneuploidy to oncogenesis. Given the current state of the field, in which we have a near-complete map of the cytogenetic, mutational and epigenetic landscape of cancer, these insights will be crucial for understanding the complex cooperation between common fusion oncogenes, recurrently mutated genes and larger amplifications or deletions during disease initiation and progression. As we illustrate with the identification of MAX as a RUNX1A co-factor and its pharmacological inhibition, this knowledge can have direct therapeutic implications.

Acknowledgements

We thank D. Trono of EFPL, Lausanne, Switzerland, for kindly providing pMD2.G (Addgene plasmid 12259) and psPAX2 (Addgene plasmid 12260) and D.E. Zhang for sharing the *RUNX1A* cDNA. Figures and visual abstract were created with BioRender.com. J.H.K receives funding from the European Research Council (ERC) under the European Union's Horizon 2020 research and innovation programme (grant agreement No 714226) and is a recipient of the St. Baldrick's Robert Arceci Innovations Award. D.H was supported by the Deutsche Krebshilfe (DKH; #111743). This work was supported by grants to J.H.K. from the German Research Foundation (DFG; KL-2374/1-3), BMBF (01GM1911D myPred) and the DKH (#109251 and #110806). S.G., M.L., F.J.S., S.K.K. and L.S. were supported by the Hannover Biomedical Research School.

Author contributions

S.G. and D.B.H. performed experiments, analyzed and interpreted data and revised the manuscript. H.I., R.B., O.A.V., L.V., A.L.S., S.L., M.L., C.I., L.S, F.J.S. and S.K.K. performed experiments and analyzed data. E.R., K.S., M.G., S.M., R.W. and M.N. performed bioinformatics analysis and data interpretation, and revised the manuscript. A.S., S.H., M.L.Y. supervised the analyses and revised the manuscript. D.R. provided patient material and data. D.H. and J.H.K. designed the study, analyzed and interpreted data, wrote the manuscript and academically drove the project.

Declaration of interests

D.R. has advisory roles for Celgene Corporation, Novartis, Bluebird Bio, Janssen, and receives research funding from CLS Behring and Roche. J.H.K. has advisory roles for

Bluebird Bio, Novartis, Roche and Jazz Pharmaceuticals. M.L.Y. is partially employed by Alacris Theranostics.

References

1. Cancer Genome Atlas Research N, Ley TJ, Miller C, et al. Genomic and epigenomic landscapes of adult de novo acute myeloid leukemia. *N Engl J Med*. 2013;368(22):2059-2074.
2. Bolouri H, Farrar JE, Triche T, Jr., et al. The molecular landscape of pediatric acute myeloid leukemia reveals recurrent structural alterations and age-specific mutational interactions. *Nat Med*. 2018;24(1):103-112.
3. Maclean GA, Menne TF, Guo G, et al. Altered hematopoiesis in trisomy 21 as revealed through in vitro differentiation of isogenic human pluripotent cells. *Proc Natl Acad Sci U S A*. 2012;109(43):17567-17572.
4. Mitelman F, Heim S, Mandahl N. Trisomy 21 in neoplastic cells. *Am J Med Genet Suppl*. 1990;7:262-266.
5. Duijf PH, Schultz N, Benezra R. Cancer cells preferentially lose small chromosomes. *Int J Cancer*. 2013;132(10):2316-2326.
6. Wechsler J, Greene M, McDevitt MA, et al. Acquired mutations in GATA1 in the megakaryoblastic leukemia of Down syndrome. *Nat Genet*. 2002;32(1):148-152.
7. Labuhn M, Perkins K, Matzk S, et al. Mechanisms of Progression of Myeloid Preleukemia to Transformed Myeloid Leukemia in Children with Down Syndrome. *Cancer Cell*. 2019;36(2):123-138 e110.
8. Yoshida K, Toki T, Okuno Y, et al. The landscape of somatic mutations in Down syndrome-related myeloid disorders. *NatGenet*. 2013;45(11):1293-1299.
9. Gurbuxani S, Vyas P, Crispino JD. Recent insights into the mechanisms of myeloid leukemogenesis in Down syndrome. *Blood*. 2004;103(2):399-406.
10. Banno K, Omori S, Hirata K, et al. Systematic Cellular Disease Models Reveal Synergistic Interaction of Trisomy 21 and GATA1 Mutations in Hematopoietic Abnormalities. *Cell Rep*. 2016;15(6):1228-1241.
11. Roy A, Cowan G, Mead AJ, et al. Perturbation of fetal liver hematopoietic stem and progenitor cell development by trisomy 21. *Proc Natl Acad Sci U S A*. 2012;109(43):17579-17584.
12. Ng AP, Hyland CD, Metcalf D, et al. Trisomy of Erg is required for myeloproliferation in a mouse model of Down syndrome. *Blood*. 2010;115(19):3966-3969.
13. Birger Y, Goldberg L, Chlon TM, et al. Perturbation of fetal hematopoiesis in a mouse model of Down syndrome's transient myeloproliferative disorder. *Blood*. 2013;122(6):988-998.
14. Malinge S, Bliss-Moreau M, Kirsammer G, et al. Increased dosage of the chromosome 21 ortholog Dyrk1a promotes megakaryoblastic leukemia in a murine model of Down syndrome. *J Clin Invest*. 2012;122(3):948-962.
15. Volk A, Liang K, Suraneni P, et al. A CHAF1B-Dependent Molecular Switch in Hematopoiesis and Leukemia Pathogenesis. *Cancer Cell*. 2018;34(5):707-723 e707.
16. Alejo-Valle O, Weigert K, Bhayadia R, et al. The megakaryocytic transcription factor ARID3A suppresses leukemia pathogenesis. *Blood*. 2021.
17. Wagenblast E, Araujo J, Gan OI, et al. Mapping the cellular origin and early evolution of leukemia in Down syndrome. *Science*. 2021;373(6551).
18. Klusmann JH, Godinho FJ, Heitmann K, et al. Developmental stage-specific interplay of GATA1 and IGF signaling in fetal megakaryopoiesis and leukemogenesis. *Genes Dev*. 2010;24(15):1659-1672.
19. Chou ST, Byrska-Bishop M, Tober JM, et al. Trisomy 21-associated defects in human primitive hematopoiesis revealed through induced pluripotent stem cells. *Proc Natl Acad Sci U S A*. 2012;109(43):17573-17578.

20. Grimm J, Heckl D, Klusmann JH. Molecular Mechanisms of the Genetic Predisposition to Acute Megakaryoblastic Leukemia in Infants With Down Syndrome. *Front Oncol*. 2021;11:636633.
21. Okuda T, van Deursen J, Hiebert SW, Grosveld G, Downing JR. AML1, the target of multiple chromosomal translocations in human leukemia, is essential for normal fetal liver hematopoiesis. *Cell*. 1996;84(2):321-330.
22. Wang Q, Stacy T, Binder M, Marin-Padilla M, Sharpe AH, Speck NA. Disruption of the Cbfa2 gene causes necrosis and hemorrhaging in the central nervous system and blocks definitive hematopoiesis. *Proc Natl Acad Sci U S A*. 1996;93(8):3444-3449.
23. North TE, de Bruijn MF, Stacy T, et al. Runx1 expression marks long-term repopulating hematopoietic stem cells in the midgestation mouse embryo. *Immunity*. 2002;16(5):661-672.
24. Kirsammer G, Jilani S, Liu H, et al. Highly penetrant myeloproliferative disease in the Ts65Dn mouse model of Down syndrome. *Blood*. 2008;111(2):767-775.
25. Liu X, Zhang Q, Zhang DE, et al. Overexpression of an isoform of AML1 in acute leukemia and its potential role in leukemogenesis. *Leukemia*. 2009;23(4):739-745.
26. Bourquin JP, Subramanian A, Langebrake C, et al. Identification of distinct molecular phenotypes in acute megakaryoblastic leukemia by gene expression profiling. *Proc Natl Acad Sci U S A*. 2006;103(9):3339-3344.
27. Ghozi MC, Bernstein Y, Negreanu V, Levanon D, Groner Y. Expression of the human acute myeloid leukemia gene AML1 is regulated by two promoter regions. *Proc Natl Acad Sci U S A*. 1996;93(5):1935-1940.
28. Fujita Y, Nishimura M, Taniwaki M, Abe T, Okuda T. Identification of an alternatively spliced form of the mouse AML1/RUNX1 gene transcript AML1c and its expression in early hematopoietic development. *Biochem Biophys Res Commun*. 2001;281(5):1248-1255.
29. Sroczynska P, Lancrin C, Kouskoff V, Lacaud G. The differential activities of Runx1 promoters define milestones during embryonic hematopoiesis. *Blood*. 2009;114(26):5279-5289.
30. Challen GA, Goodell MA. Runx1 isoforms show differential expression patterns during hematopoietic development but have similar functional effects in adult hematopoietic stem cells. *Exp Hematol*. 2010;38(5):403-416.
31. Komeno Y, Yan M, Matsuura S, et al. Runx1 exon 6-related alternative splicing isoforms differentially regulate hematopoiesis in mice. *Blood*. 2014;123(24):3760-3769.
32. Li Z, Godinho FJ, Klusmann JH, Garriga-Canut M, Yu C, Orkin SH. Developmental stage-selective effect of somatically mutated leukemogenic transcription factor GATA1. *Nat Genet*. 2005;37(6):613-619.
33. Ling T, Birger Y, Stankiewicz MJ, et al. Chromatin occupancy and epigenetic analysis reveal new insights into the function of the GATA1 N terminus in erythropoiesis. *Blood*. 2019;134(19):1619-1631.
34. Birdwell C, Fiskus W, Kadia TM, DiNardo CD, Mill CP, Bhalla KN. EVI1 dysregulation: impact on biology and therapy of myeloid malignancies. *Blood Cancer J*. 2021;11(3):64.
35. Schwarzer A, Emmrich S, Schmidt F, et al. The non-coding RNA landscape of human hematopoiesis and leukemia. *Nat Commun*. 2017;8(1):218.
36. Emmrich S, Rasche M, Schoning J, et al. miR-99a/100~125b tricistrons regulate hematopoietic stem and progenitor cell homeostasis by shifting the balance between TGFbeta and Wnt signaling. *Genes Dev*. 2014;28(8):858-874.
37. Grinev VV, Barneh F, Ilyushonak IM, et al. RUNX1/RUNX1T1 mediates alternative splicing and reorganises the transcriptional landscape in leukemia. *Nat Commun*. 2021;12(1):520.
38. Arkoun B, Robert E, Boudia F, et al. Stepwise GATA1 and SMC3 mutations alter megakaryocyte differentiation in a Down syndrome leukemia model. *J Clin Invest*. 2022;132(14).

39. Jutzi JS, Bogeska R, Nikoloski G, et al. MPN patients harbor recurrent truncating mutations in transcription factor NF-E2. *J Exp Med*. 2013;210(5):1003-1019.
40. Marcault C, Zhao LP, Maslah N, et al. Impact of NFE2 mutations on AML transformation and overall survival in patients with myeloproliferative neoplasms. *Blood*. 2021;138(21):2142-2148.
41. Elagib KE, Racke FK, Mogass M, Khetawat R, Delehanty LL, Goldfarb AN. RUNX1 and GATA-1 coexpression and cooperation in megakaryocytic differentiation. *Blood*. 2003;101(11):4333-4341.
42. Alford KA, Reinhardt K, Garnett C, et al. Analysis of GATA1 mutations in Down syndrome transient myeloproliferative disorder and myeloid leukemia. *Blood*. 2011;118(8):2222-2238.
43. Kanezaki R, Toki T, Terui K, et al. Down syndrome and GATA1 mutations in transient abnormal myeloproliferative disorder: mutation classes correlate with progression to myeloid leukemia. *Blood*. 2010;116(22):4631-4638.
44. Crossley M, Merika M, Orkin SH. Self-association of the erythroid transcription factor GATA-1 mediated by its zinc finger domains. *Mol Cell Biol*. 1995;15(5):2448-2456.
45. Shimizu R, Trainor CD, Nishikawa K, Kobayashi M, Ohneda K, Yamamoto M. GATA-1 self-association controls erythroid development in vivo. *J Biol Chem*. 2007;282(21):15862-15871.
46. Xu G, Kanezaki R, Toki T, et al. Physical association of the patient-specific GATA1 mutants with RUNX1 in acute megakaryoblastic leukemia accompanying Down syndrome. *Leukemia*. 2006;20(6):1002-1008.
47. Tijssen MR, Cvejic A, Joshi A, et al. Genome-wide analysis of simultaneous GATA1/2, RUNX1, FLI1, and SCL binding in megakaryocytes identifies hematopoietic regulators. *Dev Cell*. 2011;20(5):597-609.
48. Han H, Jain AD, Truica MI, et al. Small-Molecule MYC Inhibitors Suppress Tumor Growth and Enhance Immunotherapy. *Cancer Cell*. 2019;36(5):483-497 e415.
49. Ichikawa M, Asai T, Saito T, et al. AML-1 is required for megakaryocytic maturation and lymphocytic differentiation, but not for maintenance of hematopoietic stem cells in adult hematopoiesis. *Nat Med*. 2004;10(3):299-304.
50. Growney JD, Shigematsu H, Li Z, et al. Loss of Runx1 perturbs adult hematopoiesis and is associated with a myeloproliferative phenotype. *Blood*. 2005;106(2):494-504.
51. Senserrich J, Batsivari A, Rybtsov S, et al. Analysis of Runx1 Using Induced Gene Ablation Reveals Its Essential Role in Pre-liver HSC Development and Limitations of an In Vivo Approach. *Stem Cell Reports*. 2018;11(3):784-794.
52. Draper JE, Sroczynska P, Leong HS, et al. Mouse RUNX1C regulates premegakaryocytic/erythroid output and maintains survival of megakaryocyte progenitors. *Blood*. 2017;130(3):271-284.
53. Sakurai H, Harada Y, Ogata Y, et al. Overexpression of RUNX1 short isoform has an important role in the development of myelodysplastic/myeloproliferative neoplasms. *Blood Adv*. 2017;1(18):1382-1386.
54. Tanaka T, Tanaka K, Ogawa S, et al. An acute myeloid leukemia gene, AML1, regulates hemopoietic myeloid cell differentiation and transcriptional activation antagonistically by two alternative spliced forms. *EMBO J*. 1995;14(2):341-350.
55. Bertrand-Philippe M, Ruddell RG, Arthur MJ, Thomas J, Mungalsingh N, Mann DA. Regulation of tissue inhibitor of metalloproteinase 1 gene transcription by RUNX1 and RUNX2. *J Biol Chem*. 2004;279(23):24530-24539.
56. Guo H, Ma O, Speck NA, Friedman AD. Runx1 deletion or dominant inhibition reduces Cebpa transcription via conserved promoter and distal enhancer sites to favor monopoiesis over granulopoiesis. *Blood*. 2012;119(19):4408-4418.

57. Ran D, Shia WJ, Lo MC, et al. RUNX1a enhances hematopoietic lineage commitment from human embryonic stem cells and inducible pluripotent stem cells. *Blood*. 2013;121(15):2882-2890.
58. Alford KA, Slender A, Vanes L, et al. Perturbed hematopoiesis in the Tc1 mouse model of Down syndrome. *Blood*. 2010;115(14):2928-2937.
59. Byrska-Bishop M, VanDorn D, Campbell AE, et al. Pluripotent stem cells reveal erythroid-specific activities of the GATA1 N-terminus. *J Clin Invest*. 2015;125(3):993-1005.
60. Makishima H, Visconte V, Sakaguchi H, et al. Mutations in the spliceosome machinery, a novel and ubiquitous pathway in leukemogenesis. *Blood*. 2012;119(14):3203-3210.
61. Meers MP, Tenenbaum D, Henikoff S. Peak calling by Sparse Enrichment Analysis for CUT&RUN chromatin profiling. *Epigenetics & Chromatin*. 2019;12(1):42.

Figure Legends

Figure 1. CRISPR-Cas9 screen reveals *RUNX1* dependency in ML-DS
(A) Schema of the high-throughput Hsa21 CRISPR-Cas9 *in vitro* screen.
(B) Dot plots showing the $\log_{10}$ fold change and $-\log_{10}$ (p two-sided) of the Hsa21 sgRNAs in CMK (left), K562 (middle) and both (right; maximum likelihood estimation [MLE] β score) cell lines. Dark green dots represent highly depleting sgRNAs in CMK cells that also deplete in K562s. Light green dots represent positive controls (*MYB, MYC, ACTB, SF3B3, RPL9, POLR2A*). Blue dots represent sgRNAs targeting *RUNX1*.
(C) Dot plot showing the number of sgRNA-transduced (sgCtrl and sgRUNX1.1-1.5 indicated by shape) CMK and K562 cells (with stable Cas9 expression) after 14 days of culture normalized to day 0 (n=2 per sgRNA, two-tailed unpaired t-test).
(D) Experimental setup for evaluating *RUNX1* knockout *in vivo*. ML-DS blasts (with stable Cas9 expression) were transduced with sgRUNX1 (E2Crimson$^+$, sgRUNX1.1) or a sgCtrl (E2Crimson$^+$) and mixed 1:1 with sgCtrl-transduced blasts (GFP$^+$), before transplantation into sub-lethally irradiated recipient mice.
(E) Dot plot showing the ratio of E2Crimson$^+$ to GFP$^+$ cells after 12 days of culture normalized to day 0 (left; n=4, two-tailed unpaired t-test) and in the bone marrow of mice sacrificed 6-8 weeks after transplantation (right; n=5, Mann Whitney test).
(F) Schematic representation of the human RUNX1 genomic locus (upper panel) and the 3 main RUNX1 transcript isoforms (lower panel; not to scale). Functional exons encoding the DNA-binding domain (Runt; red) and transactivation domain (TAD; blue) are indicated. Bar graph showing RUNX1 isoform distribution (Oxford Nanopore sequencing) in polyA$^+$-enriched RNA samples from TAM and ML-DS samples.
(G) Expression of *RUNX1A* and *RUNX1C* isoforms normalized to the expression of β2-microglobulin (*B2M*) (left graph; two-way ANOVA) and *RUNX1A* to *RUNX1C* ratios (right graph; one-way ANOVA) in CD34$^+$ HSPCs, erythrocytes, megakaryocytes, granulocytes and monocytes isolated from healthy donors, as well as in leukemic blasts from TAM/ML-DS patients.

Figure 2. Increased RUNX1A:RUNX1C ratio induces malignant ML-DS phenotype
(A-C) Neonatal (top panel) and fetal (bottom panel) CD34$^+$ HSPCs were lentivirally transduced with *RUNX1A*, *RUNX1C* or empty vector (EV) control. (A) Colonies after plating CD34$^+$ HSPCs from two independent donors in methylcellulose-based CFU assays (mean±s.d., n=2; one-way ANOVA). (B) Percentage of immature (CD41$^+$CD61$^+$/CD42$^-$) and mature megakaryocytes (CD41$^+$CD61$^+$/CD42$^+$) and (C) immature CD34$^+$ cells after 7 days in media promoting megakaryocytic differentiation (mean±s.d., n=5, two-way ANOVA).
(D-F) ML-DS patient derived cells were lentivirally transduced with *RUNX1A*, *RUNX1C* or empty vector control (EV). (D) Percentage of GFP$^+$ transduced cells normalized to

day 0 post transduction (mean±s.d., n=3, one-way ANOVA, **P_{ANOVA}<0.01). Bar graphs showing the percentage of (E) $CD41^+CD117^+$ and $CD41^+CD117^-$ megakaryocytic cells or (F) $CD33^+CD117^+$ and $CD33^+CD117^-$ myeloid cells 5 days post transduction (mean±s.d., n=3, two way ANOVA).
(G) Experimental setup for evaluating RUNX1A:RUNX1C restoration *in vivo*. ML-DS blasts from two patients were transduced with *RUNX1A* (GFP^+), *RUNX1C* (GFP^+) or empty vector (EV) control (GFP^+) and mixed 1:1 with EV control-transduced blasts ($dTomato^+$), before transplantation into sub-lethally irradiated recipient mice.
(H) Ratio of GFP^+ to $dTomato^+$ cells in the bone marrow (BM) of mice sacrificed 4-8 weeks after transplantation (n=5, Kruskal-Wallis test).

Figure 3. *RUNX1A* synergizes with *Gata1s* in leukemic transformation of murine fetal liver cells.
Cas9-knock-in $Ter119^-$ FLCs were lentivirally transduced with either *Gata1* (sgGata1s) or control (sgCtrl) sgRNAs, as well as with *RUNX1A, RUNX1B, RUNX1C* or empty vector control (EV).
(A) Absolute cell number of murine FLCs after combined transduction with lentiviral vectors and maintenance in liquid cultures. Data from one representative experiment performed in replicates are shown as mean±s.d (two-way ANOVA). *P_{ANOVA}<0.05, **P_{ANOVA}<0.001; ****P_{ANOVA}<0.0001.
(B) Flow cytometry plots of murine sgGata1s+*RUNX1A*, sgGata1s+EV and sgCtrl+*RUNX1A* transduced FLCs in liquid culture. The percentage of cells belonging to each immunophenotype is indicated in the corresponding gates. Data from 3 replicates +/-s.d. are shown.
(C-D) Bar graphs showing normalized enrichment scores (NES) of significantly up- or downregulated gene sets associated with differentiation and oncogenic cellular programs, in *Gata1s*- (sgGata1s+EV, orange), *RUNX1A*- (sgCtrl+*RUNX1A*, blue) and *Gata1s*- and *RUNX1A*- (sgGATA1s+*RUNX1A*, red) murine FLCs compared to sgCtrl+EV control FLCs. This analysis highlights the unique and synergistic functional features of *Gata1s* and *RUNX1A*. *FDR q-value<0.25; **FDR q-value<0.05.
(E) Bar graph showing normalized enrichment scores (NES) of significantly up- or downregulated gene sets in *Gata1s*+*RUNX1A* (red) and *Gata1s*+*RUNX1C* (green) expressing FLCs compared to control sgCtrl+EV FLCs. This analysis highlights the contrasting functional features of *RUNX1A* and *RUNX1C* on a *Gata1s* background. *FDR q-value<0.25; **FDR q-value<0.05. .
(F-H) Analysis of mice transplanted with *RUNX1A*- or EV-transduced *Gata1s*-FLCs (n=10 per group), including comparisons of (F) Kaplan-Meier survival curves (log-rank test), (G) spleen weights (unpaired t-test), and (H) flow cytometry on bone marrow cells from the diseased mice (two-way ANOVA).
(I) Heatmap representation of RNA-seq data, showing unsupervised hierarchical clustering on the 2,824 most variable genes (standard deviation >1) across five bone

marrow samples from leukemic mice and FACS-sorted murine fetal liver HSCs [LSK ($Lin^-Sca1^+cKit^+$), common myeloid progenitors (CMP) ($Lin^-Sca1^-cKit^+CD34^+$ $CD16/32^{med}$), granulocyte-monocyte progenitors (GMP) ($Lin^-Sca1^-cKit^+CD34^+$ $CD16/32^+$), and megakaryocyte-erythroid progenitors (MEP) ($Lin^-Sca1^-cKit^+CD34^-$ $CD16/32^{low}$)]. The sample types are color-coded on the bottom of the heatmap and Z-scores are indicated by the legend at the top of the panel.
(J) Bar graph showing normalized enrichment scores (NES) of significantly up- or downregulated gene sets in the murine leukemia samples compared to all progenitor populations. *FDR q-value<0.25; **FDR q-value<0.05.

Figure 4. Distinct RUNX1A and RUNX1C protein interaction networks.
(A) Experimental setup for isolating HA-RUNX1A- or HA-RUNX1C-containing protein complexes from CMK cells.
(B) RUNX1A and RUNX1C complex composition in CMK cells with functional grouping. The Venn diagram shows significantly enriched interactors (log_2 fold change >1; p-value <0.05).
(C) Western blot confirming co-immunoprecipitation of MAX and RUNX1A using anti-MAX and anti-RUNX1 antibodies. Representative picture of 2 independent experiments using K562 cells are shown. 10% input was used as the loading control.
(D) Western blot showing RUNX1A/C isoforms co-immunoprecipitated with doxycycline-inducible HA-tagged GATA1 and GATA1s or the empty control vector. Representative picture of 3 independent experiments using CMK cells are shown. 5% input was used as the loading control.

Figure 5. RUNX1A affects gene regulation by displacing endogenous RUNX1C.
(A) Experimental setup of CUT&RUN on murine *Gata1s*-FLCs after doxycycline-induced expression of HA-RUNX1A/RUNX1C. CUT&RUN was performed using anti-HA, anti-RUNX1(C-term) and anti-GATA1 antibodies. Peaks were called by SEACR [61] using EV control cells as background. Data represent one experiment.
(B) Venn diagram showing the number of genomic regions bound by endogenous RUNX1, endogenous GATA1s and/or HA-RUNX1A after HA-RUNX1A overexpression.
(C) Heatmaps depicting the co-localization of endogenous GATA1s (orange, left), endogenous RUNX1 (green, middle), and HA-RUNX1A/-RUNX1C (red, right) signals after doxycycline-induced HA-RUNX1A or HA-RUNX1C expression in Gata1s-FLCs. Empty vector (EV) transduced cells were used as a control. Regions ±2.5 kb of the peak center are shown. Binding intensities are represented normalized rpkm values (bars below the blots).
(D) Binding intensities (normalized read density) of RUNX1 (left) and GATA1s (right), in EV control and doxycycline-induced HA-RUNX1A and HA-RUNX1C expressing cells.
(E) Transcription factor motif enrichment analysis under RUNX1 peaks, at the promoter regions of genes that are differentially expressed upon doxycycline induced RUNX1A

expression (log_2 FC = 1). Human promoter regions were used as background. Z-score intensities are shown.
(F) IGV snapshots of *Mxd1* and *Lyl1* gene promoters showing occupancy of endogenous GATA1s, RUNX1 and HA-RUNX1A/-RUNX1C in *Gata1s*-FLCs after doxycycline induced HA-RUNX1A/-RUNX1C expression or in EV control expressing cells. The tracks display coverage (RPKM) (left). Scale and chromosome location are shown (top).

Figure 6. Interfering with MYC:MAX dimerization as a therapeutic strategy
(A-B) Dose response curves for MYC:MAX dimerization inhibitor MYCi361 in *Gata1s*-FLC cells (A, left) and in ML-DS blasts derived from three patients (B, left) 24h after treatment *in vitro*. Corresponding IC_{50}-values are depicted below the graphs. Bar graphs showing the percentage of AnnexinV$^+$ cells after treatment with the indicated doses of MYCi361 in comparison to the DMSO control in *Gata1s*-FLCs (A, right) and in ML-DS blasts (B, right); data represented as mean ± SD (n=3; one-way ANOVA).
(C) Experimental setup for evaluating MAX dependence in ML-DS and AMKL cells *in vivo*. ML-DS or AMKL blasts derived from two patients were transduced with *shMAX* (GFP$^+$) or shCtrl (GFP$^+$) and mixed 1:1 with shCtrl-transduced blasts (dTomato$^+$), before transplantation into sub-lethally irradiated recipient mice.
(D) Ratio of GFP$^+$ to dTomato$^+$ cells in the bone marrow (BM) of mice sacrificed 4-8 weeks after transplantation (n=5, Kruskal-Wallis test).

Figure 1

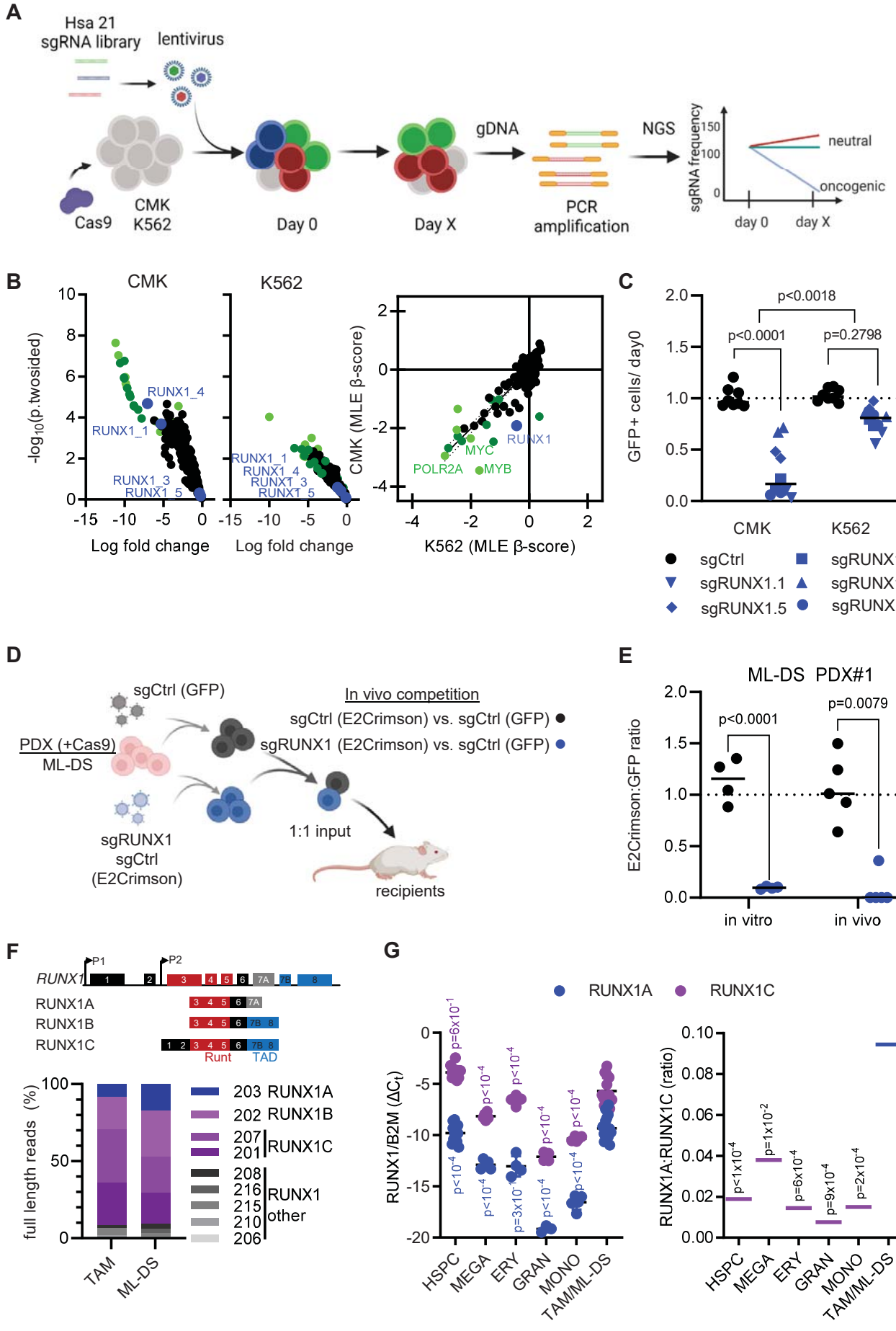

Figure 2

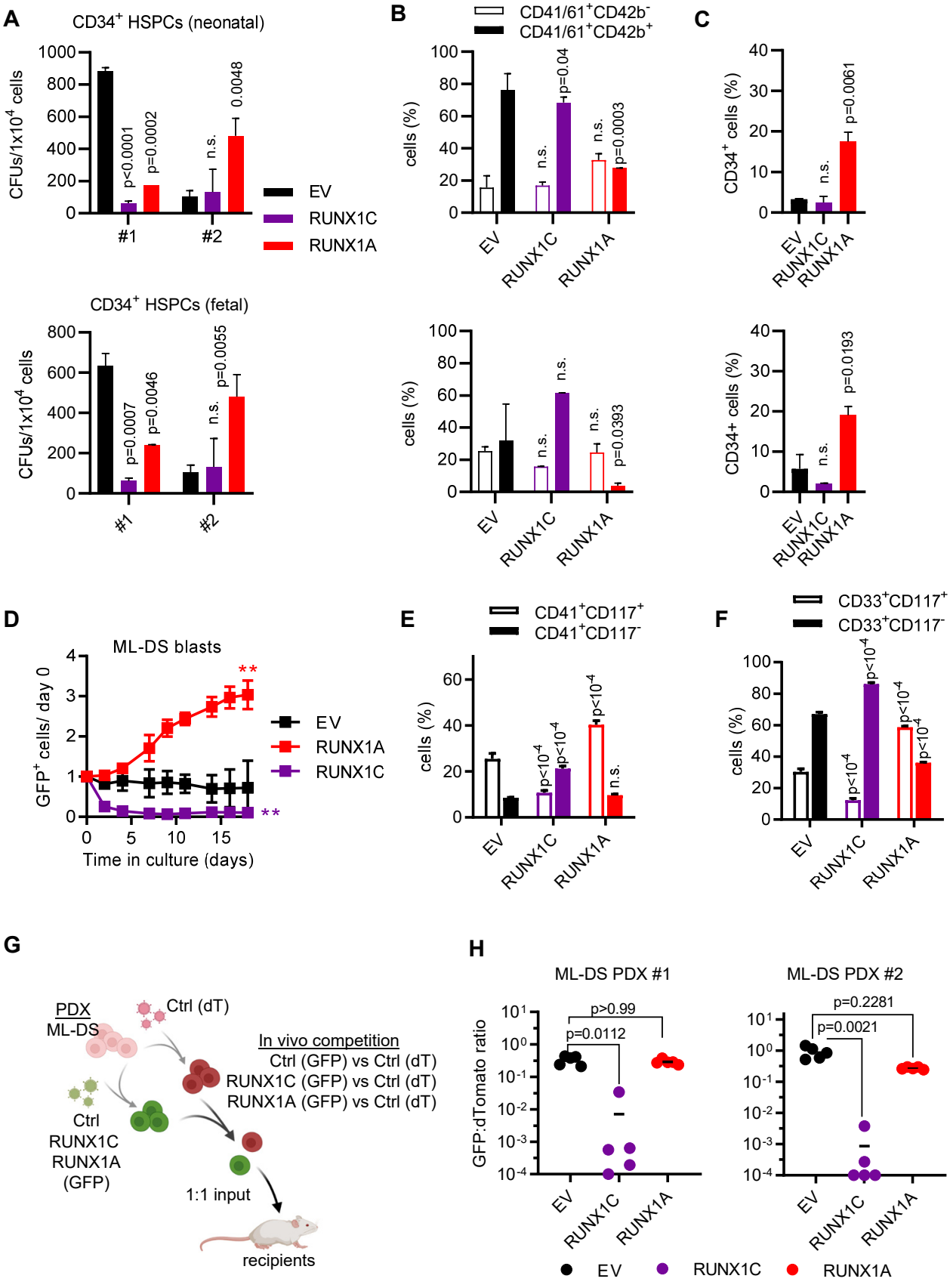

Figure 3

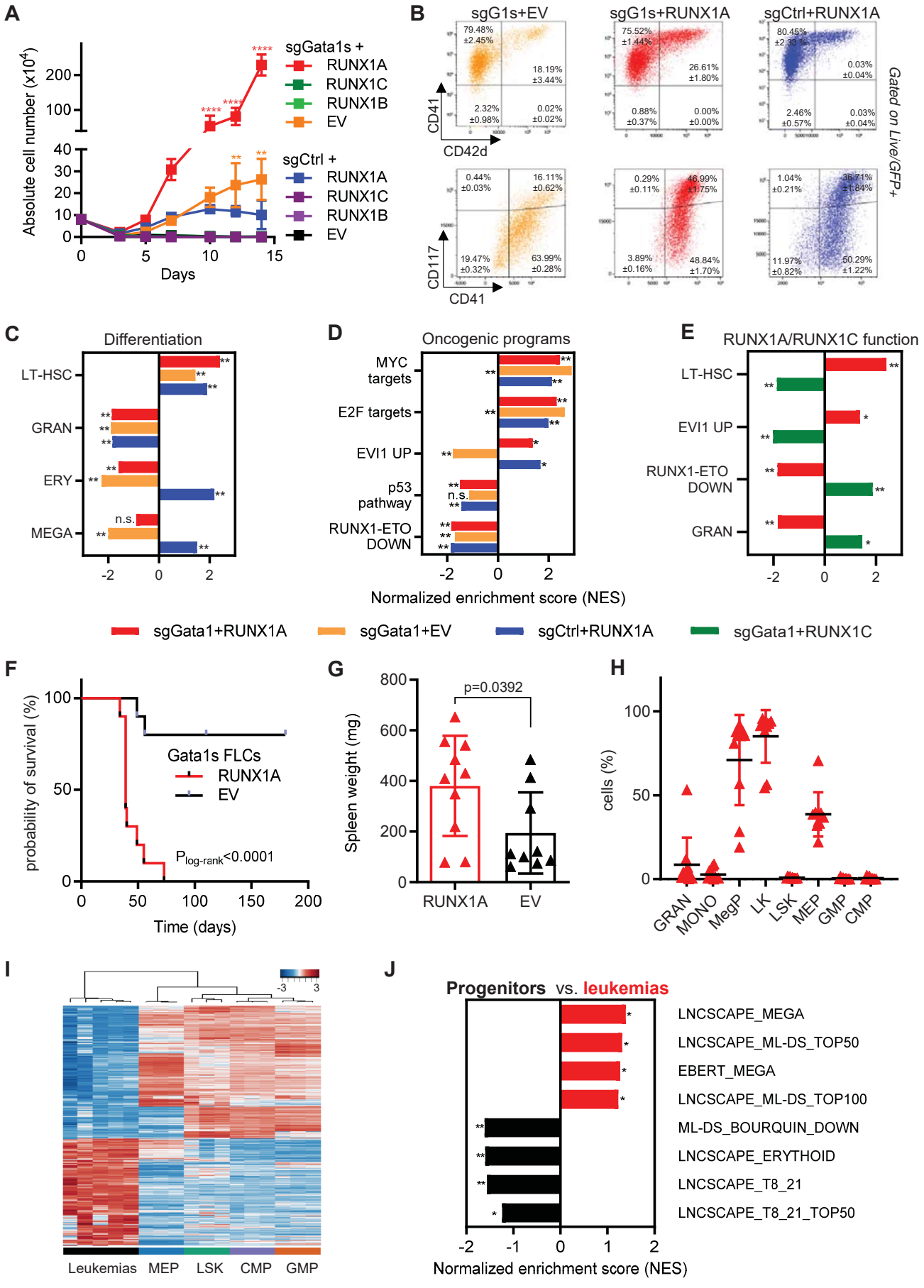

Figure 4

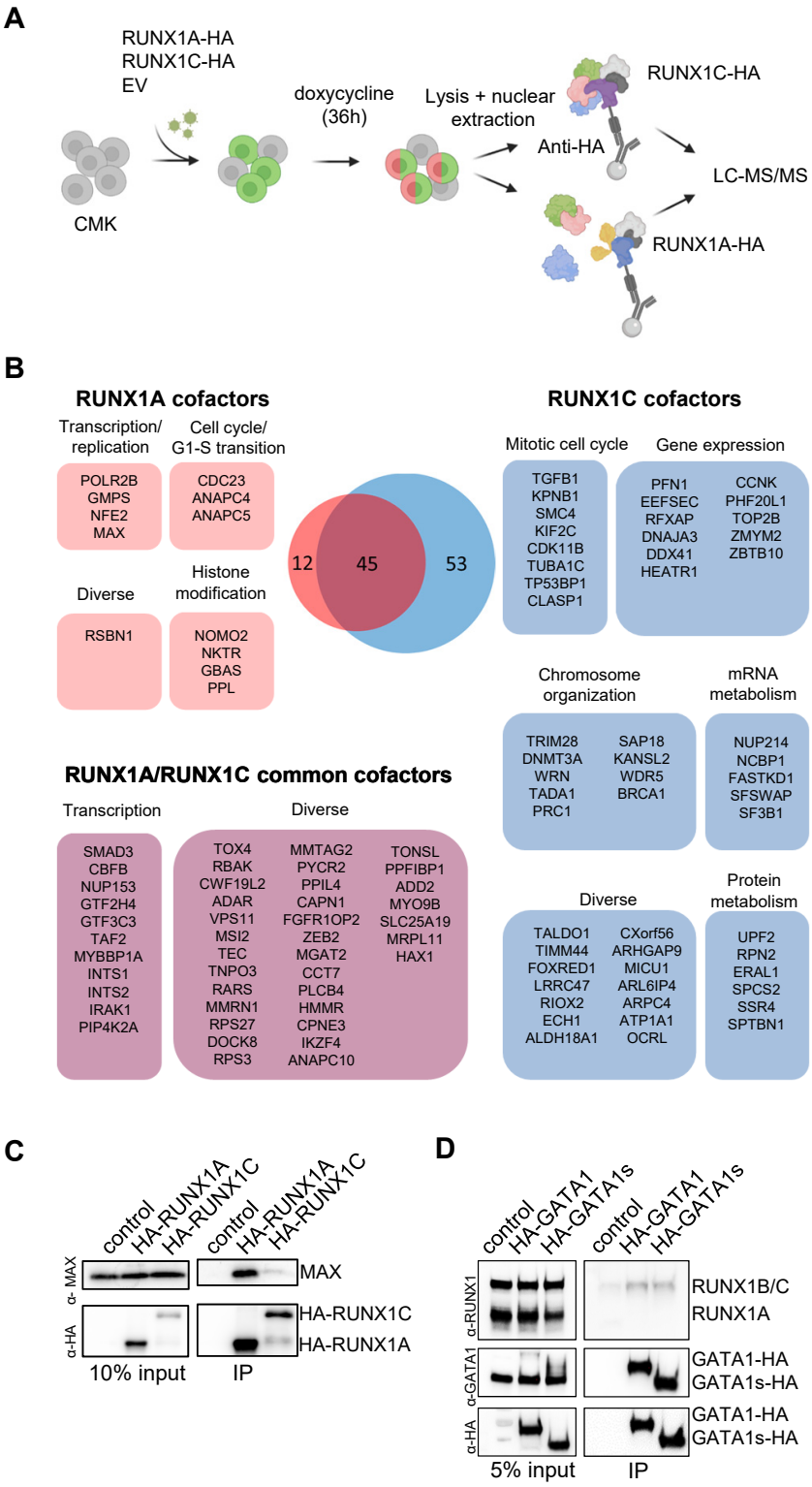

Figure 5

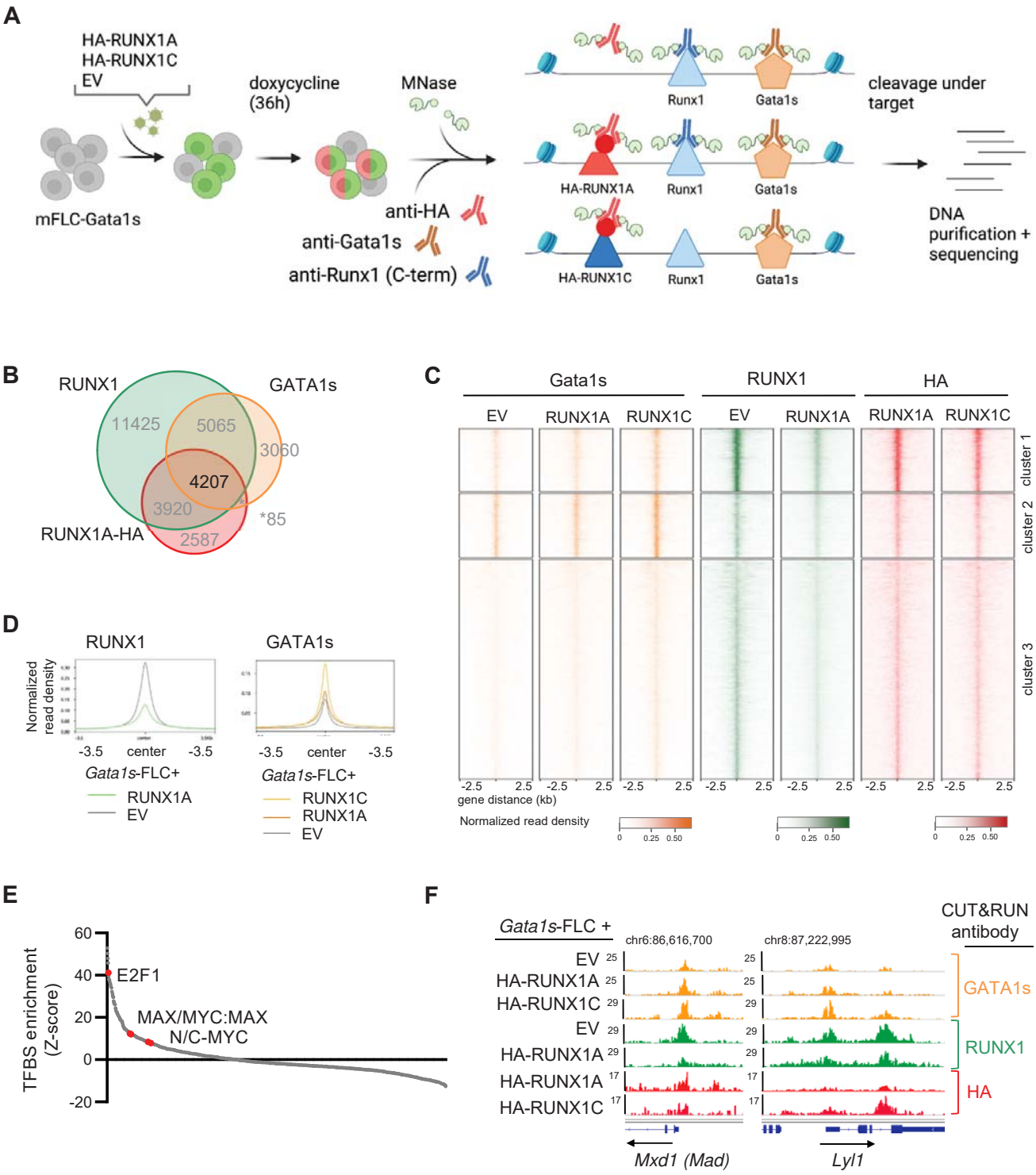

Figure 6